Ultrasonic Irradiation on Hydrolysis of Magnesium Hydride to Enhance Hydrogen Generation

Shun Hiroi, Sou Hosokai, Tomohiro Akiyama

Center for Advanced Research of Energy and Materials, Faculty of Engineering,

Hokkaido University, Sapporo 060-8628, Japan

Corresponding author: Phone: +81-11-706-6842; Fax: +81-11-726-0731.

E-mail address: takiyama@eng.hokudai.ac.jp (Tomohiro Akiyama)

Abstract:

This paper describes the ultrasonic irradiation on the hydrolysis of magnesium hydride to enhance hydrogen generation; the effects of the ultrasonic frequency and the sample size on the hydrogen generation were mainly examined. In the experiments, three MgH_2 particle and nanofiber samples were soaked in distilled water and ultrasonically irradiated at frequencies of 28, 45, and 100 kHz. Then, the amount of hydrogen generated was measured. We found that the low frequency of ultrasonic irradiation and the relatively small sample size accelerated the hydrolysis reaction $MgH_2 + 2H_2O = Mg(OH)_2 + 2H_2 + 277$ kJ. In particular, the MgH_2 nanofibers exhibited the maximum hydrogen storage capacity of 14.4 mass% at room temperature at a frequency of 28 kHz (ultrasound irradiation). The results also experimentally validated that a combination of ultrasonic irradiation and MgH_2 hydrolysis is considerably effective for efficiently generating hydrogen without heating and adding any agent.

Keywords: Hydrogen generation, Hydrogen storage material, Magnesium hydride, Hydrolysis, Ultrasonic irradiation, Nanofiber

1. Introduction

Hydrogen storage materials have attracted considerable attention among the modern scientific community [1–3] because hydrogen is the most promising candidate for energy carriers [4]. In particular, magnesium hydride, MgH_2, has been drawing worldwide attention for several reasons: abundant resource, low-cost performance, light weight, safety, and a large hydrogen storage capacity of 7.6 mass% [5–8]. However, temperatures higher than 300°C are required for the hydrogen desorption reaction, $MgH_2 \rightarrow Mg + H_2$, because of a thermodynamic restriction [1, 3, 9]. In fact, such a high dissociation temperature limits the practical use of MgH_2 as a hydrogen storage medium.

An alternative route for producing hydrogen using MgH_2 is the hydrolysis of MgH_2 [10–18] (1) as follows:

$$MgH_2 + 2H_2O \rightarrow Mg(OH)_2 + 2H_2, \qquad \Delta H^{o}_{298} = -277 \text{ kJ} \qquad (1)$$

This route does not require a heating process like the hydrogen dissociation reaction of $MgH_2 \rightarrow Mg + H_2$ because hydrogen is thermodynamically generated even at room temperature, together with exothermic heat. Then, the actual hydrogen storage density increases from 7.6 mass% to 15.2 mass% on the basis of the weight of MgH_2 since hydrogen comes from not only magnesium hydride but also water. The only demerit of

this route is that the reaction, given by equation (1), is irreversible. For materializing this route, we need to design an additional Mg cycling process after the hydrolysis; in this process, the regeneration technology of magnesium hydroxide to magnesium/magnesium hydride, such as the carbothermic reduction of MgO + C = Mg + CO − 491 kJ using biomass, is also under investigation.

Switching back to the route of Mg hydrolysis, we recognize that this route is kinetically slow for a practical application; that is, the hydrolysis of MgH_2 is rapidly interrupted by the formation of a passive magnesium hydroxide, $Mg(OH)_2$, layer onto the unreacted MgH_2 core. To overcome this problem, several methods have been proposed thus far [12-17]. As an example of the physical methods, ball milling with salts was effective in exfoliating the $Mg(OH)_2$ layer and pulverizing particles. This is explained by the accentuation of the pitting corrosion due to the creation of numerous defects and fresh surfaces through the milling process. In addition, simply, the use of hot water was a practical solution to increase the rate of MgH_2 hydrolysis. As a chemical method, the charging of additives, such as the buffering agent, chelator, and ion exchanger, was also helpful for the hydrolysis of MgH_2 due to the lack of the formation of an $Mg(OH)_2$ layer, even if the additives behaved as impurities in the post-Mg cycling process. Above methods greatly contributed to the elucidation of the

kinetics of MgH_2 hydrolysis, although the rate was still not considerably large.

Sonication has been widely applied to many chemical and physical processes for activating various phenomena, such as the acceleration of a chemical reaction, emulsification, degassing, and extraction, using ultrasonic irradiation [19-23]. An important feature of an ultrasound is the *cavitation*, which consists of the formation, growth, and collapse of micro bubbles. The cavitation can result in drastic local conditions of very high temperatures (thousands of degrees) and pressures (more than tens of atmospheres) [19]. In spite of its significance, the effect of ultrasound irradiation on the hydrolysis of MgH_2 has never been reported as yet. Therefore, the purpose of this research project is to study the ultrasonic irradiation on the hydrolysis of magnesium hydride to enhance hydrogen generation; in this study, the effects of the ultrasonic frequency and the sample size on the hydrolysis rate were mainly examined. The results revealed that an ultrasound will enhance the hydrolysis reaction of MgH_2 by increasing reaction rate constant due to the generation of radical and exfoliating the passive layer of $Mg(OH)_2$ over the unreacted MgH_2 due to the generation of large shear forces.

2. Experimental

2.1. Sample

Figure 1 shows the SEM images of three samples used in this study. Two commercially available, (a) large MgH_2 particles and (b) small MgH_2 particles with (average size, purity) = (60 μm, 99 mass%) and (2 μm, 90 mass%), were prepared by carrying out a *gas-solid reaction* (GSR) under specified conditions of temperature and pressure. Further, we produced (c) an MgH_2 nanofiber, having a diameter of 500 nm and length of several tens of microns by using *hydriding chemical vapor deposition* (HCVD) [24-26]. During HCVD, magnesium hydride was deposited on the inconel substrate via a gas phase reaction between magnesium vapor and high-pressure hydrogen. The detailed procedure is described elsewhere [24-26].

Table 1 gives the physical characteristics of the abovementioned three samples; these characteristics were determined using X-ray diffraction with Cu-Kα radiation (XRD, Miniflex, Rigaku Co., Ltd.), a scanning electron microscope (SEM, Japan Electron Co., Pty.), and a nitrogen adsorption method (Autsorb 6AG, Yuasa Ionics Co., Pty.). Note that the small sample had a large specific surface area, as expected.

2.2. Hydrolysis experiments

Figure 2 shows a schematic representation of the experimental setup for the hydrolysis of the MgH_2 samples. The setup consists of two parts: a hydrolysis reactor and a hydrogen collector. The former is a flask with an inner volume of 300 cm^3 and has 0.1 g of the MgH_2 sample; this flask was placed in an ultrasonic bath (W-113 SANPA, Honda Electronics Co., Ltd., ultrasonic intensity is 100 W), and temperatures in the reactor and ultrasonic bath were monitored by using thermistors. The latter is a measuring cylinder with an inner volume of 250 cm^3; this cylinder was completely filled with water and placed in a water bath before the experiment. The hydrolysis reactor and the hydrogen collector were connected with a flexible Teflon tube having an inner diameter of 2 mm and length of 1100 mm. On the basis of the water substitution method, the transient hydrogen generation was evaluated from the volume and temperature data. Volume changes were monitored by a naked-eye observation at intervals of 30 s from 0 to 300 s, of 60 s from 300 to 600 s, of 120 s from 0.6 to 1.8 ks, and of 600 s from 1.8 to 7.2 ks. The reaction degree can be calculated by using the following equation:

$$\text{Reaction degree, } f\,(\%) = \frac{V_{H_2} P M_{MgH_2}}{2\Theta_{MgH_2} W_{MgH_2} RT} \times 100 \qquad (2)$$

Here, V_{H_2}, P, M_{MgH_2}, W_{MgH_2}, Θ_{MgH_2}, R, and T indicate the measured gas volume (m^3), gas pressure (Pa), molecular mass of the MgH_2 sample ($kgkmol^{-1}$), weight of the MgH_2 sample (kg), fractional purity of MgH_2 (-), gas constant (=8.314 $Jmol^{-1}K^{-1}$), and gas temperature (K), respectively.

To examine the effect of the ultrasonic frequency on the hydrolysis reaction, three frequencies of 28, 45, and 100 kHz were selected to irradiate the reactor. As soon as the experiment was begun, 5.0 cm^3 of distilled water, heated up to 25°C in advance, was introduced into the reactor. During the experiment, the hydrogen generation was monitored. After the experiments, the solid materials and solution in the reactor were recovered and filtrated; the materials obtained were identified by X-ray diffraction (XRD) and observed by using a scanning electron microscope (SEM).

3. Results and discussion

3.1. Dependence on ultrasonic frequency

Figure 3 shows the reaction curves and the temperature changes in the reactor when the samples of large MgH_2 particles (60-GSR) were sonicated at different ultrasonic frequencies. The effect of the ultrasound on the reaction curve was considerably significant; that is, a non-sonicated MgH_2 sample may generate a small amount of hydrogen only at the initial stage. However, the generation stopped immediately because of the formation of a passive magnesium hydroxide layer on the unreacted MgH_2, as expected. In contrast, sonicated MgH_2 samples continued to generate hydrogen because of a collision between the samples and the generation of surface damage by micro jets. Interestingly, the reaction degree depended drastically on the ultrasonic frequency. The large hydrolysis rate was observed when the frequencies were 28, 45, and 100 kHz. The hydrolysis rate reached as high as 76% in terms of the reaction degree at 7.2 ks at an ultrasonic frequency of 28 kHz. This value was more than 15 times the value obtained in the case of the non-sonicated sample, indicating an equivalent hydrogen density of 11.6 mass% on the basis of the weight of MgH_2. At the same time, water temperatures increased gradually when the ultrasound was irradiated because the hydrolysis is an exothermic reaction and a part of the ultrasound energy

changes to the thermal energy of water.

Figure 4 shows the XRD patterns of large MgH_2 samples (60-GSR) that were sonicated at ultrasonic frequencies of 28, 45, and 100 kHz. All the recovered samples showed only peaks of MgH_2 with/without $Mg(OH)_2$, and the intensity ratio of $Mg(OH)_2/MgH_2$ increased gradually with a decrease in frequency. This can be well explained by the fact that a large reaction degree, *f*, was obtained at a low ultrasonic frequency, as shown in Fig.3. The results also indicated that the reaction has a negligible intermediate product such as Mg and MgO, and it is simply described by MgH_2 (s) + $2H_2O$ (l) → Mg $(OH)_2$ (s) + $2H_2$ (g). The broadening of the $Mg(OH)_2$ peaks observed at 38° or 52° implied that the product had low crystallinity.

3.2. Dependence on sample species

Figure 5 shows the reaction curves of the three samples with/without sonication at ultrasonic frequencies of 28 kHz. All sonicated samples exhibited acceleration in the hydrolysis rate, and the final yield at 7.2 ks was increased by 2.4 to 30 times, as compared to that in the case of the non-sonicated samples. Except the final yield, the comparative analysis of a non-sonicated sample and a sonicated one from the viewpoint of the initial reaction rate before the formation of a passive $Mg(OH)_2$ layer is scientifically significant. Table 2 gives the comparison of the initial reaction rates, in the

unit of 10^{-6} mol $s^{-1}m^{-2}$, between the non-sonicated and sonicated samples, which were mainly evaluated from both the BET specific surface area (see Table 1) and the initial reaction curves from 0 to 30 s. We confirmed that sonication at a frequency of 28 kHz accelerated the initial reaction rate by 1.4 to 2.8 times. The large MgH_2 particle (60-GSR) sonicated at an ultrasonic frequency of 28 kHz exhibited the highest reaction rate among the three samples. The sample of the MgH_2 nanofiber (0.5-HCVD) exhibited the largest yield at 7.2 ks; however, its initial reaction rate per specific surface area was the smallest among the three samples. This could be attributed to its high crystallinity because, in general, highly crystalline materials have poor reactivity. In conclusion, the use of the MgH_2 nanofiber as an energy transportation medium was most effective from the viewpoint of hydrolysis kinetics. This was mainly attributed to the wide surface area of 14.1 m^2g^{-1} and not the intrinsic reaction rate.

Moreover, the hydrolysis rate of the sonicated samples strongly depended on the sample shape. A small sample induced a large reaction rate in the order of 0.5-HCVD, 2-GSR, and 60-GSR. This was the same as the order of the BET surface area. The reaction degree of the MgH_2 nanofiber (0.5-HCVD) at 7.2 ks reached 94.5%. This value corresponded to an equivalent hydrogen density of as much as 14.4 mass% on the basis of the weight of MgH_2. Figure 6 shows the XRD patterns of the three

sonicated samples at an ultrasonic frequency of 28 kHz; these samples were recovered at 7.2 ks. All of the peaks agreed with the two compounds of MgH_2 and $Mg(OH)_2$ perfectly according to equation (1) of the MgH_2 hydrolysis reaction. It was reasonable to conclude that with an increase in the reaction degree, the peaks of MgH_2 shortened and those of $Mg(OH)_2$ grew gradually.

Fig. 7 shows a schematic representation of the micro bubble formation, growth, and collapse under ultrasonic irradiation, in which a hot spot of high temperature and high pressure induced radical reactions and large shear forces. Remember that the indication of the thermometer is transient scatter in Fig.3. This was definitely due to the locally generated cavitation. The cavitation will enhance the hydrolysis reaction because the radical reactions increase the hydrolysis reaction rate and the large shear forces exfoliate the passive $Mg(OH)_2$ layer. For high-frequency sound waves, the time required to create the bubble may be longer than that available during the rarefaction cycle. Greater cavitation was generated at a lower ultrasonic frequency [27]. This is a reason why the ultrasonic irradiation at the frequency of 28 kHz was most effective for improving the hydrolysis kinetics, as compared to the other frequencies of 45 and 100 kHz.

4. Conclusion

We investigated the ultrasonic irradiation on the hydrolysis of magnesium hydride to enhance hydrogen generation. The particles and nanofiber of MgH_2 were prepared; introduced into water; and irradiated with frequencies of 28, 45, and 100 kHz at room temperature; then, the transient hydrogen generation was measured. The results obtained are as follows:

1) Ultrasonic irradiation was considerably effective in enhancing the hydrolysis of MgH_2. A low frequency resulted in a high hydrolysis rate due to the collision between the particles and the generation of the surface damage by micro jets. In addition, the gradual temperature rise due to the transformation from ultrasound to thermal energy accelerated the hydrolysis.

2) A small sample induced a large hydrolysis rate because of the large specific surface area. The nanofiber of MgH_2 with a diameter of 500 nm exhibited the largest hydrolysis rate. This was mainly attributed to the wide surface area of 14.1 m^2g^{-1} and not the intrinsic reaction rate.

3) The combination of the MgH_2 nanofiber and ultrasound irradiation at an ultrasonic frequency of 28 kHz was the best for the hydrolysis kinetics to produce hydrogen.

This technology will accelerate the practical use of MgH_2 as an energy carrier,

offering many benefits for transporting hydrogen easily, efficiently, and safely, by eliminating the use of additives, minimizing processing time, and encouraging the recycling of a pure $Mg(OH)_2$ product.

References

[1] Sakintuna B., Lamari-Darkrim F., & Michael H. Metal hydride materials for solid hydrogen storage: A review. *Int. J. Hydrogen Energy* **32,** 1121–1140 (2007).

[2] Chen P. & Zhu M. Recent progress in hydrogen storage. *Materials Today* **11,** 36–43 (2008).

[3] Schlapbach L. & Züttel A. Hydrogen-storage materials for mobile applications. *Nature* **32,** 353–358 (2007).

[4] Jain I. P. Hydrogen the fuel for 21st century. *Int. J. Hydrogen Energy* **34,** 7368–7378 (2009).

[5] Malka I. E., Czujko T. & Bystrzycki J. Catalytic effect of halide additives ball milled with magnesium hydride. *Int. J. Hydrogen Energy* **35,** 1706-1712 (2010).

[6] Barcelo S., Rogers M., Grigoropoulos C. P. & Mao S. S. Hydrogen storage property of sandwiched magnesium hydride nanoparticle thin film. *Int. J. Hydrogen Energy* **35,** 7232–7235 (2010).

[7] Chaise A., Rango P. de, Marty Ph., Fruchart D., Miraglia S., Olivès R. & Garrier S. Enhancement of hydrogen sorption in magnesium hydride using expanded natural graphite. *Int. J. Hydrogen Energy* **34,** 8589–8596 (2009).

[8] Chaise A., Rango P. de, Marty Ph. & Fruchart D. Experimental and numerical study of a magnesium hydride tank. *Int. J. Hydrogen Energy* **35,** 6311–6322 (2010).

[9] Poh C. K., Guo Z., & Liu H. K. Real-time measurement of desorption temperature and kinetics of magnesium hydride powder sample based on optical reflection. *Int. J. Hydrogen Energy* **34,** 9168–9172 (2009).

[10] Kong V. C. Y., Foulkes F. R., Kirk D. W., & Hinatsu J. T. Development of hydrogen storage for fuel cell generators. I: Hydrogen generation using hydrolysis hydrides. *Int. J. Hydrogen Energy* **24,** 665–675 (1999).

[11] Kojima Y., Suzuki K. I., & Kawai Y. Hydrogen generation by hydrolysis reaction of magnesium hydride. *J. Materials Science* **39,** 2227–2229 (2004).

[12] Huot J., Liang G., & Schulz R. Magnesium-based nanocomposite chemical hydrides. *J. Alloys Compd.* **353,** L12–L15 (2003).

[13] Tessier J. P., Palau P., Hout J., Schulz R., & Guay D. Hydrogen production and crystal structure of ball milled MgH_2-Ca and MgH_2-CaH_2 mixtures. *J. Alloys Compd.* **376,** 180–185 (2004).

[14] Grosjean M. H. & Roué L. Hydrolysis of Mg-salt and MgH_2-salt mixtures prepared by ball milling for hydrogen production. *J. Alloys Compd.* **416,**

296–302 (2006).

[15] Grosjean M. H., Zidoune M., Roué L., & Huot J. Y. Hydrogen production via hydrolysis reaction from ball-milled Mg-based materials. *Int. J. Hydrogen Energy* **31,** 109–119 (2006).

[16] Grosjean M. H., Zidoune M., & Roué L. Hydrogen generation via alcoholysis reaction using ball-milled Mg-based materials. *Int. J. Hydrogen Energy* **31,** 1159–1163 (2006).

[17] Lukashev R. V., Yakovleva N. A., Klyamkin S. N., & Tarasov, B. P. Effect of mechanical activation on the reaction of magnesium hydride with water. *Russ. J. Inorg. Chem.* **53,** 343–349 (2008).

[18] Makhaev V. D., Petrova L. A., & Tarasov B. P. Hydrolysis of magnesium hydride in the presence of ammonium salts. *Russ. J. Inorg. Chem.* **53,** 858–860 (2008).

[19] Ares J. R., Leardini F., Díaz-Chao P., Bodeaga J., Fernández J. F., Ferrer I. J., & Sánchez C. Ultrasonic irradiation as a tool to modify the H-desorption from hydrides: MgH_2 suspended in decane. *Ultrason. Sonochem.* **16,** 810–816 (2009).

[20] Kimura T., Fujita M., Sohmiya H., & Ando T. Ultrasonic acceleration of iodination of unactivated aliphatic hydrocarbons. *Ultrason. Sonochem.* **9,**

205–207 (2002).

[21] Tuulmets A., Salmar S., & Hagu H. Effect of ultrasound on ester hydrolysis in binary solvents. *J. Phys. Chem. B* **107,** 12891–12896 (2003).

[22] Salmar S., Cravotto G., Tuulmets A., & Hagu H. Effect of ultrasound of the base-catalyzed hydrolysis of 4-nitrophenyl acetate in aqueous ethanol. *J. Phys. Chem. B* **110,** 5817–5821 (2006).

[23] Chave T., Nikitenko S.I., Granier D., & Zemb T. Sonochemical reactions with mesoporous alumina. *Ultrason. Sonochem.* **16,** 481–487 (2009).

[24] Saita I., Toshima T., Tanda S., & Akiyama T. Hydriding chemical vapor deposition of metal hydride nano-fibers. *Mater. Trans.* **47,** 931–934 (2006).

[25] Saita I., Toshima T., Tanda S., & Akiyama T. Hydrogen storage property of MgH_2 synthesized by hydriding chemical vapor deposition. *J. Alloys Compd.* **446–447,** 80–83 (2007).

[26] Zhu C., Hayashi H., Saita I., & Akiyama T. Direct synthesis of MgH_2 nanofibers at different hydrogen pressures. *Int. J. Hydrogen Energy* **34,** 7283–7290 (2009).

[27] Mason T. J. & Lorimer J. P. *Sonochemistry Theory, Application and Uses of Ultrasound in Chemistry* (John Wiley & Sons, New York, 1988) 27–35.

Table 1 Physical characteristics of three MgH_2 samples used in this study.

Sample No.	Shape	Average Size (μm)	Purity (mass%)	BET specific surface area (m^2g^{-1})
60-GSR	particle	60	99	3.42
2-GSR	particle	2	90	8.03
0.5-HCVD[1]	nanofiber	0.5	>99	14.1

[1]This was reported to be a single crystal on the basis of an electron beam observation.

Table 2 Initial reaction rate, dF/dt, of three MgH_2 samples with/without sonication.

Sample No.	60-GSR	2-GSR	0.5-HCVD
(a) Non-sonicated	10.0	6.72	2.44
(b) Sonicated (28 kHz)	13.8	12.0	6.75
(b)/(a)	1.38	1.79	2.77

Unit: 10^{-6} mol $s^{-1}m^{-2}$. The value of dF/dt was averaged from 0 to 30 s.

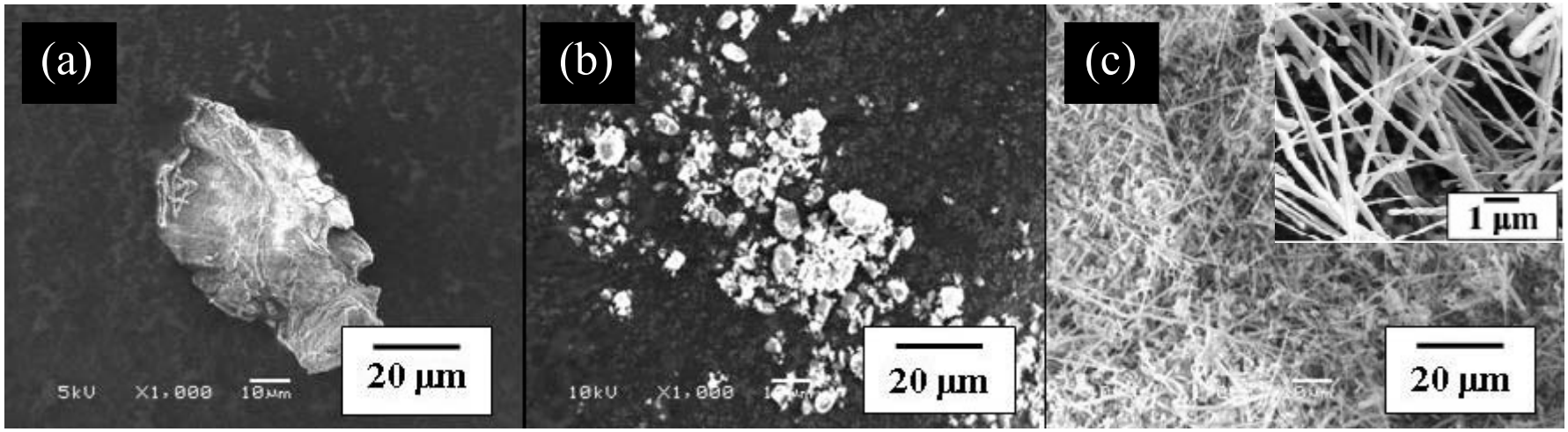

Fig. 1 SEM image of the three samples prepared:
(a) (b)GSR-MgH_2 particle which was produced from gas-solid reaction at controlled temperature and pressure by $Mg(s) + H_2(g) \rightarrow MgH_2(s)$. Nominal particle size is 60 μm in (a), 2 μm in (b)
(c) HCVD-MgH_2 nanofiber with 500 nm in diameter and several tens of microns in diameter, which was produced by *hydriding chemical vapor deposition* (HCVD) at hydrogen pressure of 4MPa by $Mg(g) + H_2(g) \rightarrow MgH_2(s)$.

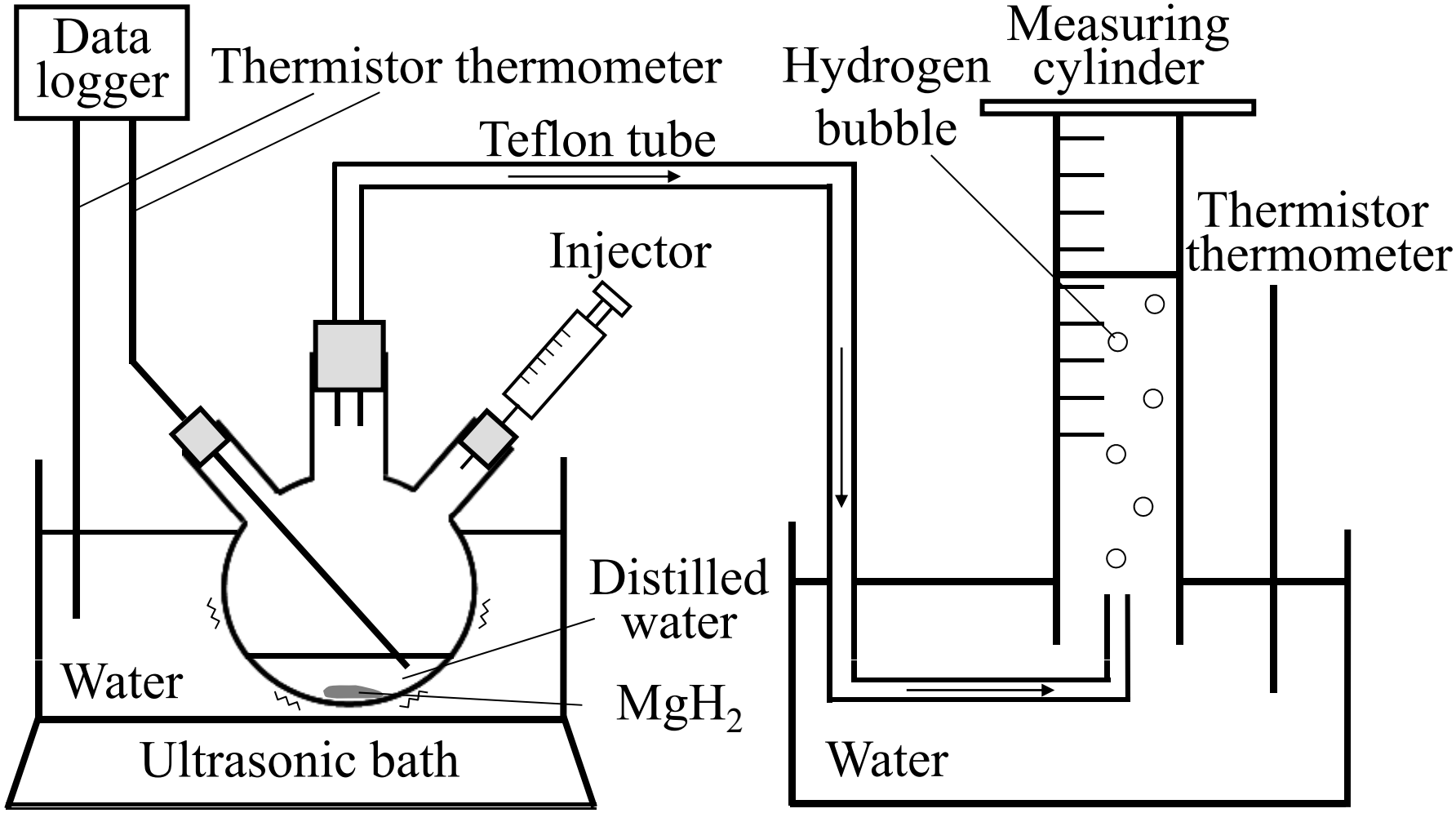

Fig. 2 Schematic diagram of the experimental setup for the hydrolysis of MgH_2, in which the experiments started by adding distilled water of 5 cm^3 to MgH_2 samples of 0.1g at 25 ^oC and the hydrogen evolution was monitored by a water substitution method.

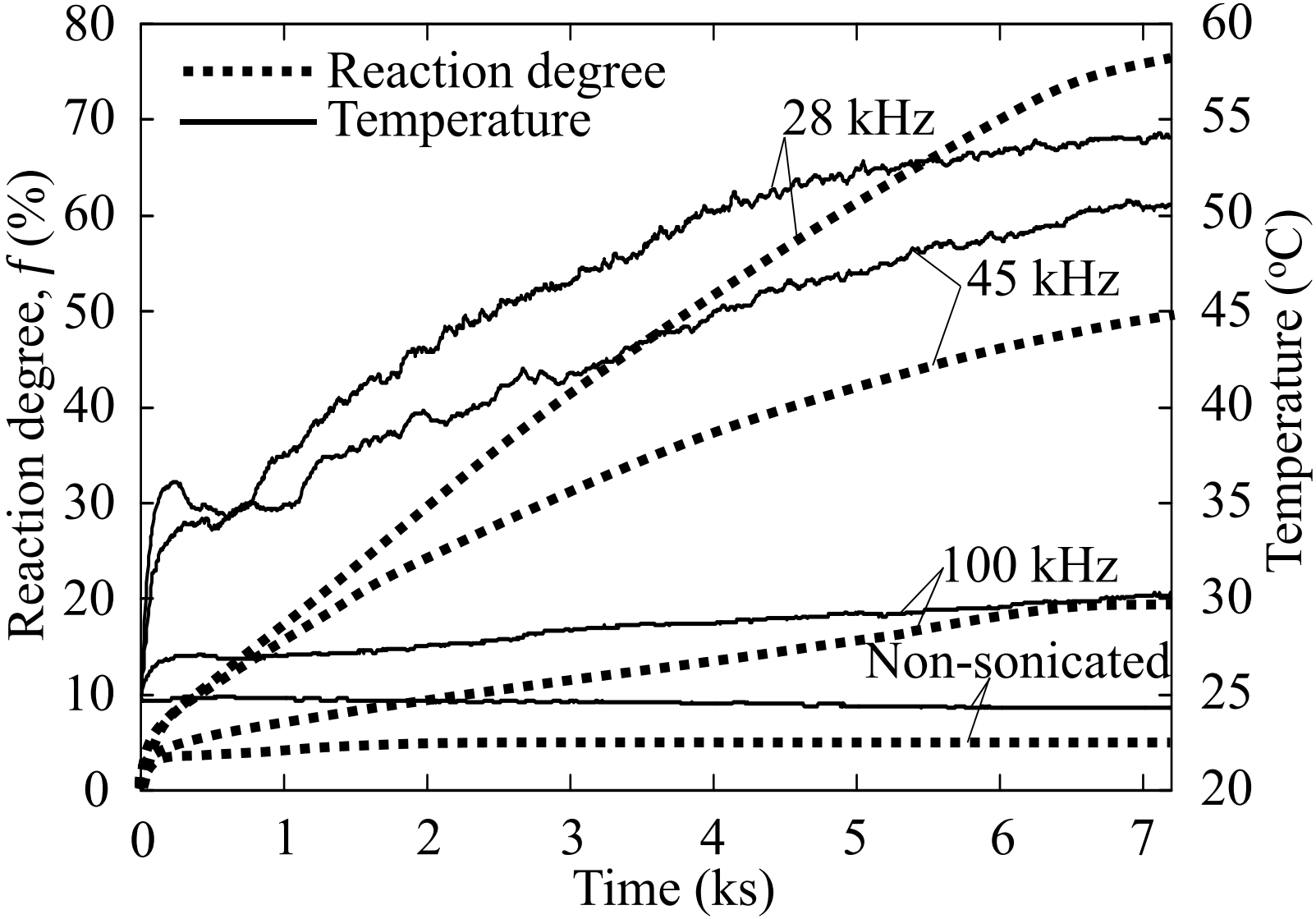

Fig. 3 Changes in hydrogen yield and sample temperature with time under the different conditions of ultrasonic frequency, in using 0.1g of 60-GSR-MgH_2. The phase of samples, which were recovered at 7.2ks, was identified by XRD analysis.

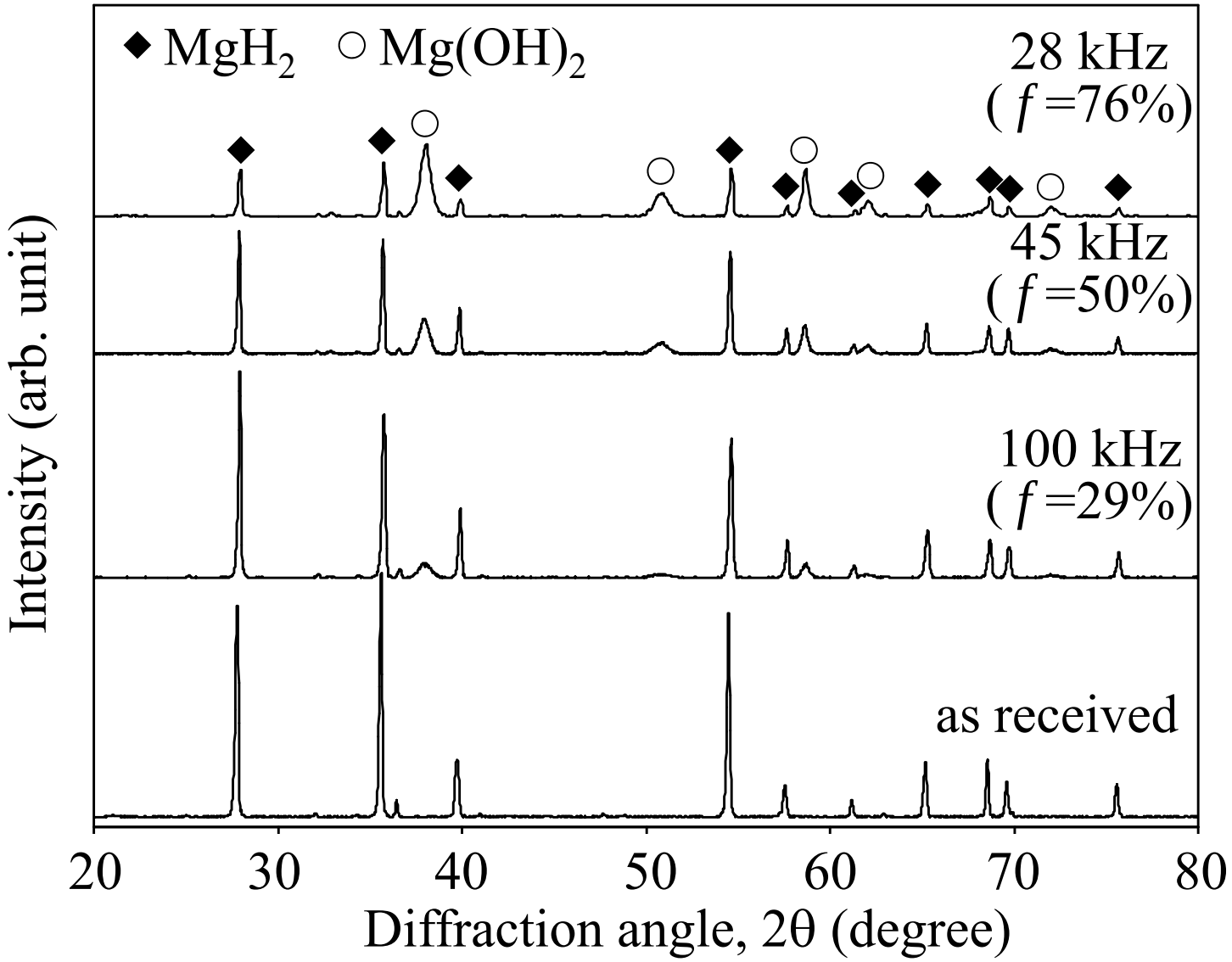

Fig. 4 Effect of ultrasonic frequency on the remaining sample of 60-GSR-MgH_2 at 7.2ks. The XRD pattern of each sample shows that the smaller frequency caused the more $Mg(OH)_2$ as product.

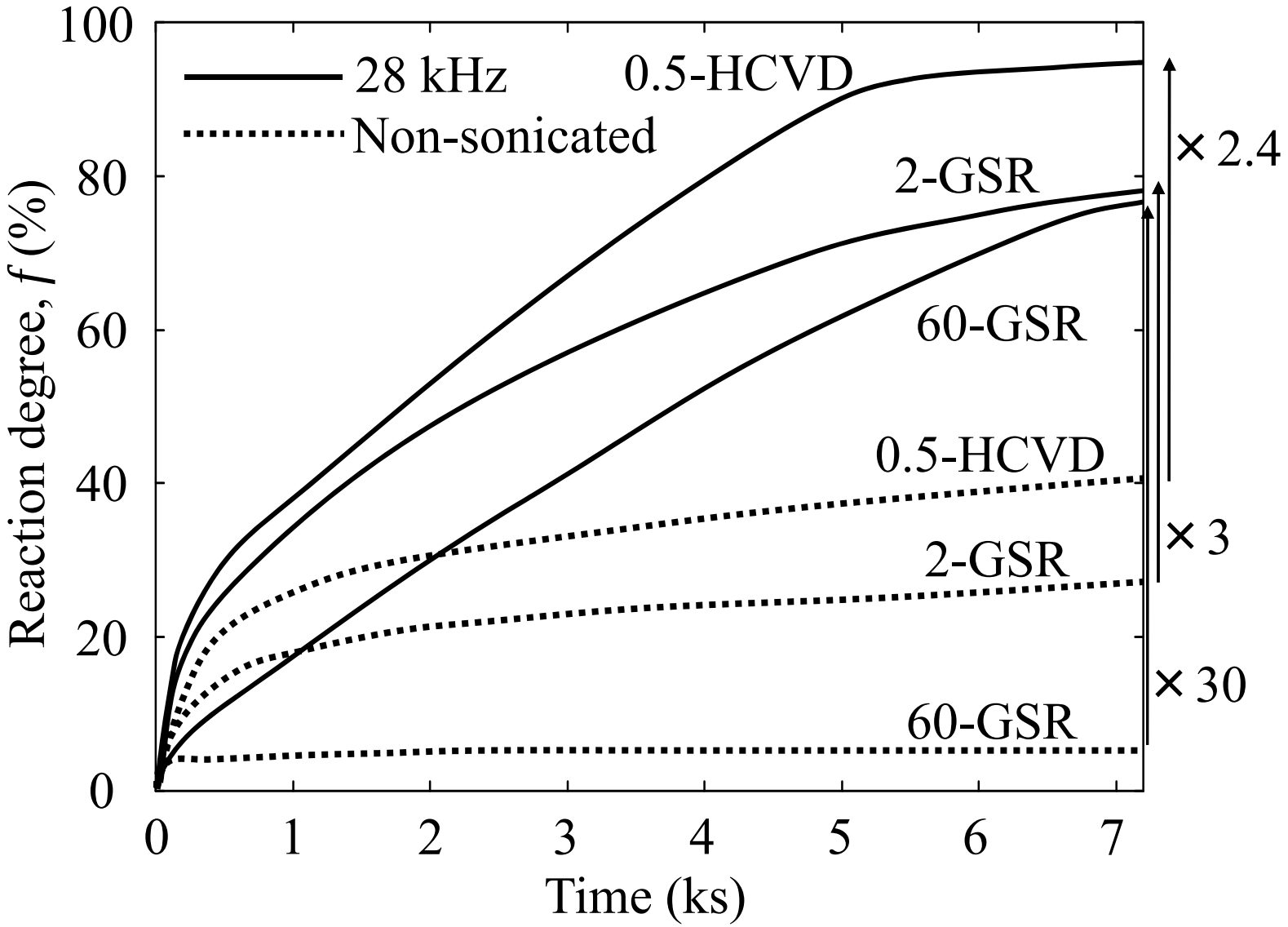

Fig.5 Effect of sample shape on reaction curves with/without sonication at ultrasonic frequency of 28 kHz.

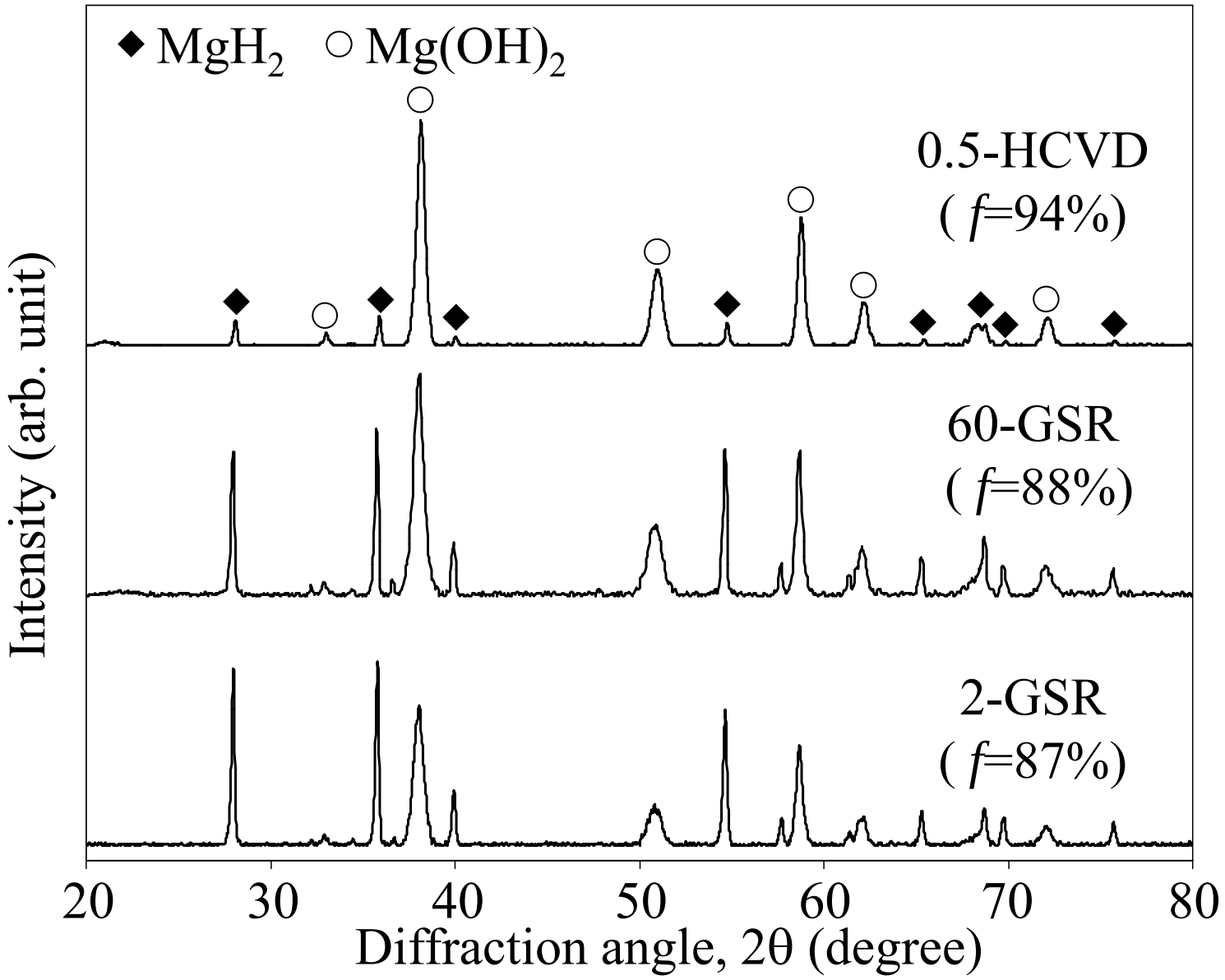

Fig. 6 X-ray diffraction patterns of three sonicated samples at ultrasonic frequency of 28 kHz, which were recovered at 7.2ks.

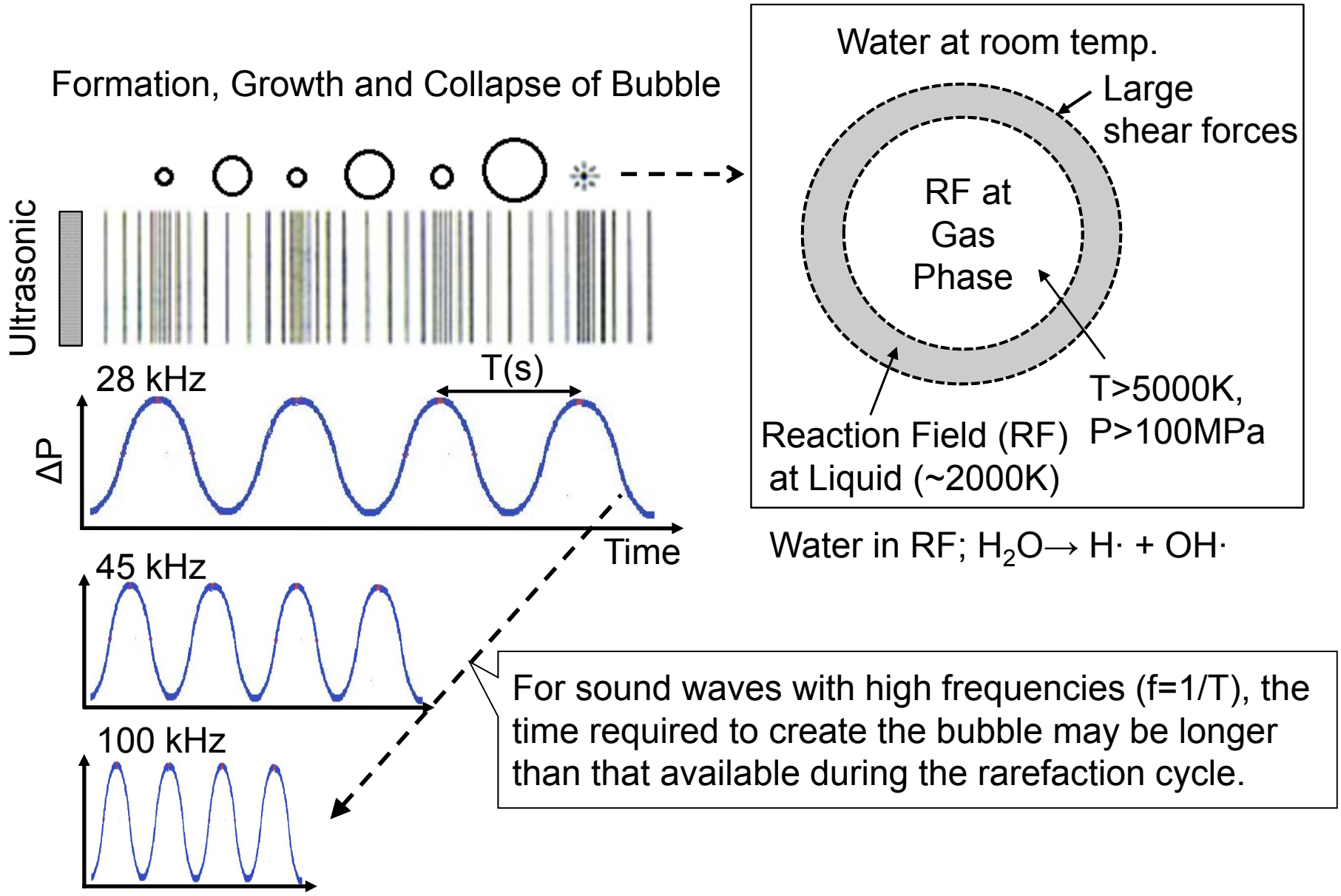

Fig.7 Schematic representation of bubble formation, growth and collapse under ultrasonic irradiation, in which hot spot induces radical reactions.